The Relationship between Vibration Level and Minimum Detectable Defect Size in Sonic-IR Inspection

Marco MORBIDINI, Peter CAWLEY, Imperial College London, UK
Tim BARDEN, Darryl ALMOND, University of Bath, UK
Philippe DUFFOUR, University College London, UK

Abstract. Sonic-IR (also called thermosonics) is attracting increasing interest as an NDT method for the detection of contacting interface-type defects such as fatigue cracks in metals and delaminations in composites. A high power acoustic horn is typically used to excite a complex vibration field which causes the defect interfaces to rub and dissipate energy as heat. The resulting local increase in temperature at one of the specimen surfaces can then be measured by an infrared camera. In this study a set of steel beams with fatigue cracks of different depth and variable partial crack opening was tested. Each beam was instrumented with strain gauges across the crack and at the back face for the measurement of both the "breathing" behaviour of the cracks and the excited vibration. The heat released at the crack was predicted from the measured vibration and an experimental estimate of the additional damping introduced in the specimens by each crack. These calculations were then used to predict the surface temperature rise as a function of time during the excitation and the results compared with the infrared camera measurements. The relationship between the crack size and the level of vibration required for reliable detection was discussed.

1. Introduction

Thermal NDE techniques have been an active subject of research since the late 70s [1]. Sonic-IR (or thermosonics) is an emerging thermal NDE method which is based on detecting the heat generated by cracks and delaminations when a powerful ultrasonic excitation is applied to the test structure. Although a vibro-thermal NDE technique was pioneered in the early 80s [2, 3], successful practical implementations of thermosonics have been reported from the late 90s [4, 5, 6]. The use of acoustic welders (acoustic resonators with typical resonance frequency at 20 or 40 kHz) has proven effective to excite high vibration amplitudes so that the amount of heat generated at the defect could be large enough to result in a detectable surface temperature rise (thermosonic signal) using commercially available infra red (IR) cameras. Small cracks in metallic specimens, having a high conductivity coefficient, have been detected [5]. The nonlinearity at the coupling between the test specimen and the acoustic horn typically results in the excitation of harmonics and sub-harmonics of the driving frequency [5, 7]. When a large number of such frequency components are excited, acoustic "chaos" can be reached and this sort of broadband excitation has been demonstrated to enhance the thermosonic signal [5, 7].

Researchers have recently put effort into understanding the mechanisms of generation of acoustic "chaos" obtained using conventional acoustic horns, and have investigated the consequent improvement in the defect detection [8]. However, more quantitative and

systematic work is still needed for thermosonics to become a fully reliable NDE technique and this study proposes a further step in this direction.

1.1 A New Approach for the Prediction of the Thermosonic Signal

The aim of this paper is to predict the thermosonic signal for a measured vibration level, and therefore to establish the vibration amplitude threshold required for a defect to be detected. For this study a set of 7 fatigue-cracked mild steel beams was used, and their geometry is shown in Figure 1 (thickness of 10 mm). The cracks were obtained by three-point bending and had variable depths from approximately 1 to 4 mm.

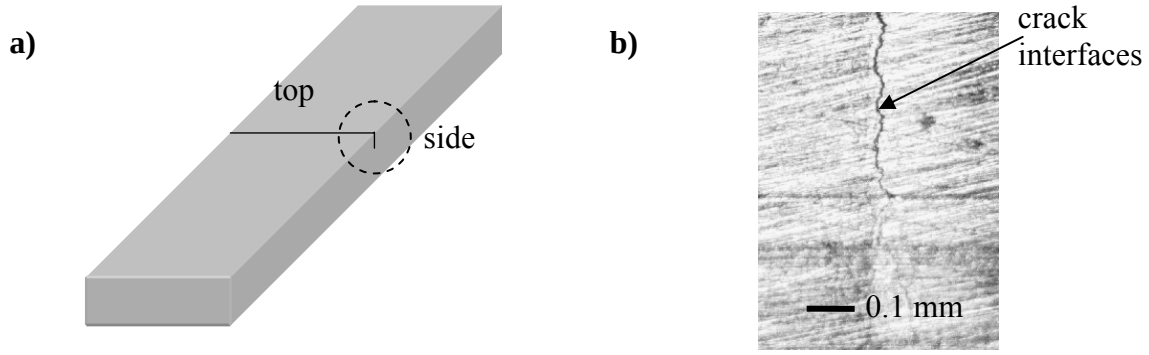

Figure 1 Schematic showing the crack in each of the 7 specimens used in the experiments (a) and picture (taken using magnification optics) showing one crack seen from the side (b).

The prediction process (represented in Figure 2) involves 2 logical steps: (1) calculating the heat released *at the crack* when the specimen is vibrated and (2) obtaining the resulting temperature rise *at the surface* (thermosonic signal) by heat propagation.

The heat produced at the crack was determined indirectly using independently measured vibration damping data. Vibration damping represents the global loss of energy in a vibrating system [9]. It has long been known that the presence of a crack in a specimen means additional damping is introduced and this can be used as a NDT method on its own [10]. From the thermosonics point of view, this extra-damping is localized *at the crack* and it is responsible for the local dissipation of energy into heat. The calculation of the heat released at the crack is therefore possible if the extra damping at the crack and the vibration of the specimen have both been characterized. This is represented in the flow chart of Figure 2 by respectively the upper and middle horizontal branches. The third horizontal branch was necessary to model the crack as a rectangular heat source uniform across the crack and non-uniform over its depth.

The resulting temperature increase at the monitoring surface (top of crack, see Figure 1) was successively obtained by inputting the calculated heat released at the crack to simple thermal models of the cracks and the beams. Such predictions were finally compared to the experimental temperature rise measured by the IR camera.

2. Damping Measurements

The additional damping introduced by the crack was measured for the 3rd flexural mode of the beams at around 3 kHz. The specimens were supported on taut strings and vibrations excited by impacting a 15-mm-diameter steel ball close to the nodes of the 1st and 5th flexural modes. The vibration decay was measured by a laser vibrometer pointed

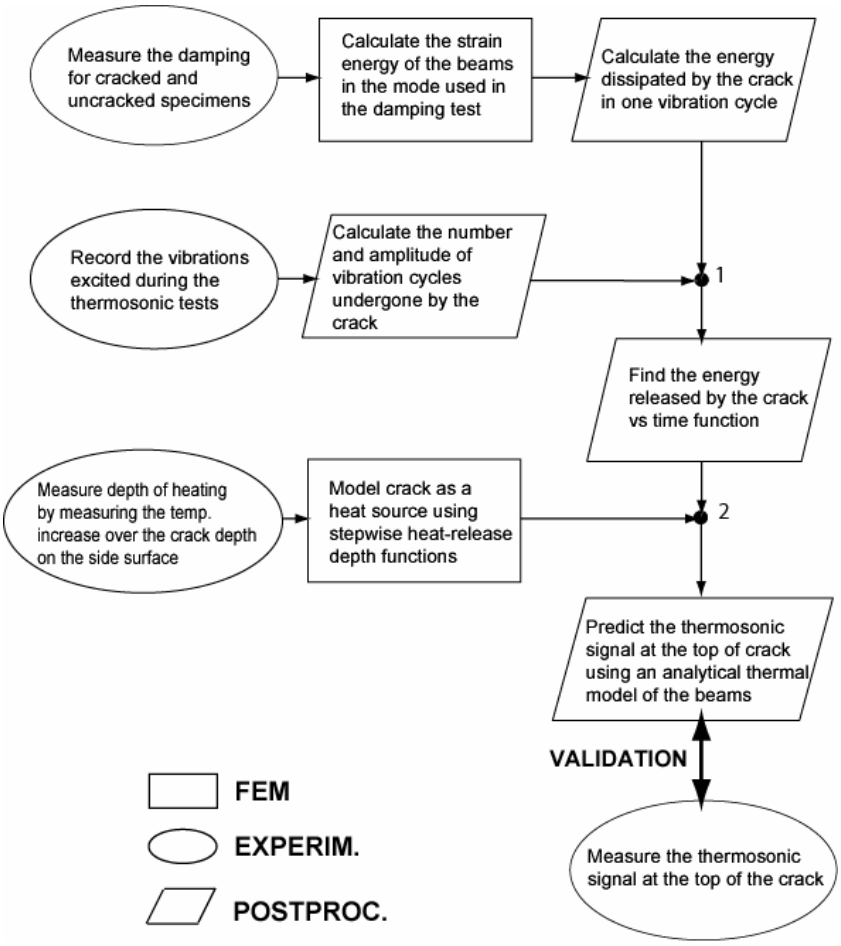

Figure 2 Block diagram showing the prediction and validation algorithm

next to the crack in the out-of-plane direction, and then recorded. Since the vibration "pick-up" was at the middle of the beams, the contribution from any excited even flexural modes was negligible as they have a node at mid-span. The excitation position was chosen so that mode 3 dominated the received signal. The recorded waveforms were analyzed in the time-frequency domain allowing the modes of the structure to be separated in frequency while their decay was measured in time. Figure 3 shows the loss factors η for each beam plotted against the vibration amplitude in micro-strain (με) measured at the back face of the crack. The bottom line in Figure 3 is the uncracked reference beam for baseline damping subtraction. The additional damping due to the presence of the crack was calculated as:

$$\eta_{crack} = \eta_{cracked} - \eta_{uncracked} \tag{1}$$

The loss factors were in general agreement with the crack severity observed by visual inspection. For beams 1 and 5 the damping tended to decrease with increasing amplitude whereas for specimen 6 it tended to increase. For all other beams no significant variation of damping with vibration amplitude was observed. Since the back-face strain is a measure of the curvature of the beams at their middle during vibration, and hence of the degree of crack opening (mode I of fracture mechanics), we assumed the crack damping independent of frequency/mode if considering odd-number flexural vibrations of the beams [11, 12]. This assumption set the basis for a time domain computation of the heat dissipated by the crack during the sonic-IR tests as illustrated by the branches in Figure 2 joining at node 1.

The thermosonic vibration could be divided into individual vibration cycles each of which was contributing to heat dissipation according to the definition of loss factor:

$$\Delta U_i = 2\pi\eta_{crack}V \tag{2}$$

where ΔU is the energy released during the cycle "i" and V is the strain energy of the beam in the 3rd flexural mode at the strain amplitude measured in the cycle "i".

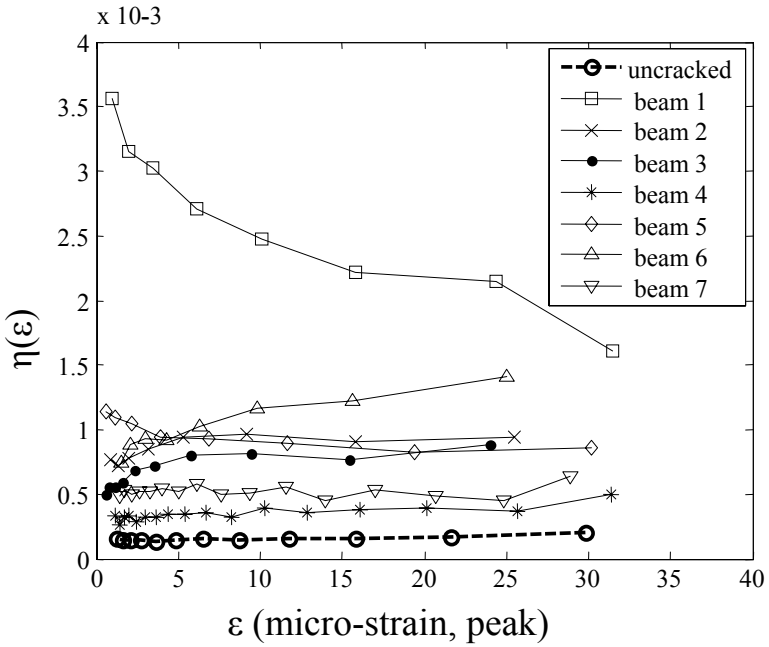

Figure 3 Loss factors as a function of back face strain. These values were measured exciting the 3rd flexural mode of the beams.

3. Sonic-IR Testing

A picture of the experimental setup is shown in Figure 4. The beams were supported against 2 vertical posts, using a G-clamp at one end and at the other by pressing the ultrasonic horn (40 kHz) against it. The odd flexural modes have antinodes at the damage site in the middle of the beams and so are the most important. Each beam was instru-

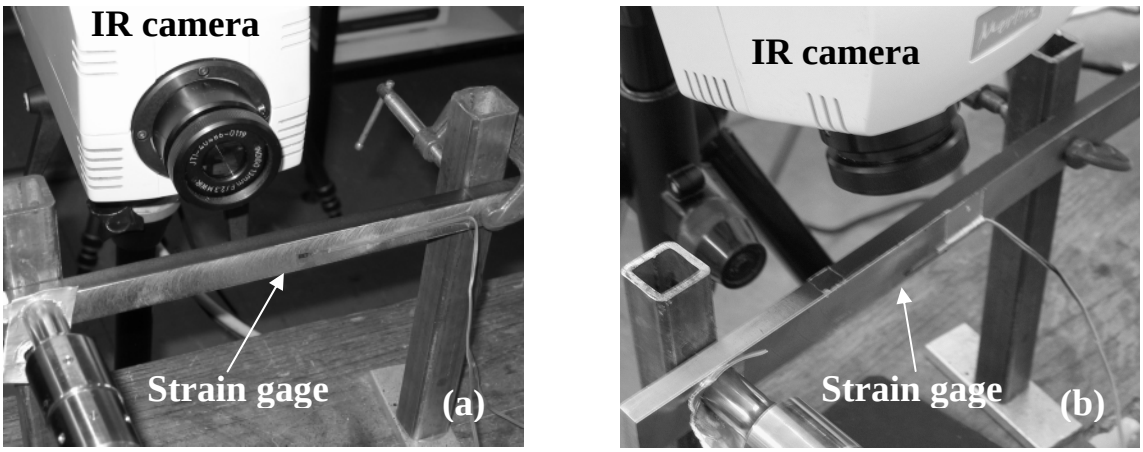

Figure 4 (a) thermosonic testing with camera pointing at the crack top. (b) thermosonic testing with camera looking at the crack side to estimate the heat distribution vs depth.

mented with a strain gage bonded precisely at the back of the crack and the pulsed vibrations (around 0.5 second) recorded for each test. Figure 5 a) shows the time trace of a typical strain signal. Multiple tests (at least 15) were conducted on each cracked beam varying the coupling conditions by repeatedly releasing the exciter and pressing it against the beams again. The maximum peak strain amplitude was typically in the interval between 10 and 100 με. During the pulse, the vibration is highly non-stationary (inserts a/1 and a/2 in Figure 5 a)) and this is due to the crude coupling between the horn and the structure.

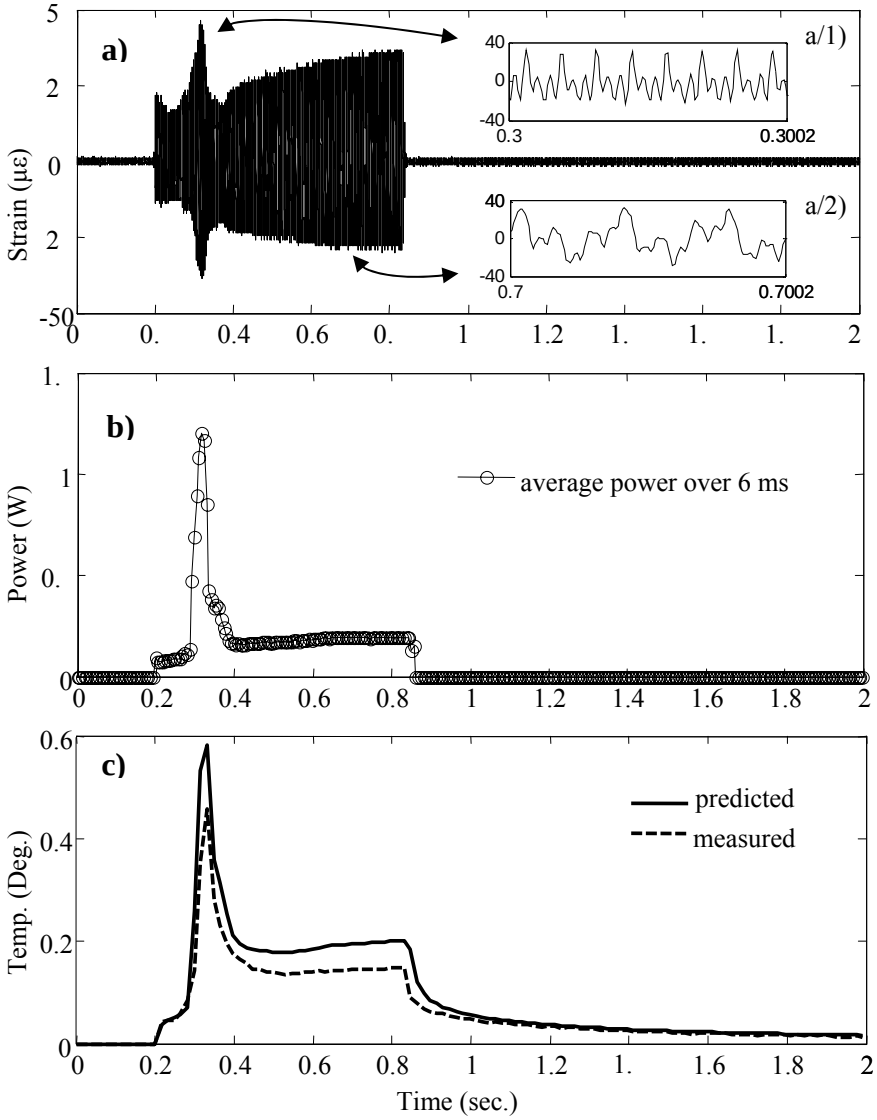

Figure 5 (a) strain record for test n 5 on specimen 1; the inserts a/1 and a/2 show different vibration regimes. (b) average power generated at the crack plotted versus time. (c) predicted and measured temperature rise on the top of the crack (average over the crack width)

One vibration cycle was defined by three consecutive `zero crossings of the recorded vibrational strain with the two halves of the cycle having strain of opposite sign. The heat liberated by the crack in one cycle was calculated using equation (2) and then averaged within time windows of 6 ms (corresponding to approximately 240 cycles at the fundamental excitation frequency of 40 kHz) to find the equivalent power liberated at the crack vs time function shown in Figure 5 b). In order to enable the use of an analytic model of heat propagation the crack had to be modelled as a simple heat source. The simplest models such as heating at the crack tip (uniform linear heat source) and uniform heating over the crack

sides (rectangular heat source) are not likely to be realistic. The cracks were modelled as heat sources on the basis of the measurement of the heat released at the cracks over their depth as shown in Figure 4 b). The power dissipated was assumed to be a stepwise function of the crack depth. This is equivalent to considering the crack as the superposition of two or more rectangular sources of uniform power, each located at a different depth over the crack. Such stepwise functions (one for each crack) were found by fitting the temperature rise measured at the crack side (setup shown in Figure 4 b)) at the onset of the vibration, when the effects of heat diffusion were almost negligible. In order to do this, a thermal finite element (FE) iterative analysis was carried out, where an initially assumed heat-release step function was iteratively updated to give a FE temperature profile along the crack side that fitted the measured temperature profile. The temperature rise at the side of the cracks was only measured a few times for each beam in order to estimate the heat-release step functions. All the other tests were conducted measuring the temperature rise at the top of the cracks across their width. This was the standard testing configuration.

The aim of this paper is to predict the temperature rise observed by the IR setup in the standard configuration, on the basis of the damping measurements and the measurement and analysis of the strain recorded at the back face of the crack. This was achieved by using the model of the crack as heat source described in the previous paragraph, using the principle of superposition. Since the crack was described as a finite number of rectangular sources of uniform power embedded in the beam at different depths over the cracked cross section, the temperature rise at the top of crack was the sum of the temperature rises caused by each rectangle separately. The problem of finding the surface temperature rise when a rectangular heat source is embedded in the material can be solved numerically and has been already used in thermosonics [13]. In this paper, adiabatic conditions at the surfaces were used and no lateral heat flow (no edge effects) was also assumed, given the geometry of the cracked specimens. It is finally important to recall that the power dissipated at the crack is function of time, as explained earlier. This feature was also incorporated in the thermal modelling by effectively considering the heat-release step functions as time varying proportionality coefficients. In this way, the heat-release depth functions could describe the actual power dissipated at the crack in time. However the assumption was made that the step functions calculated at the beginning of pulse would still be valid throughout the whole pulse duration.

3.1 Comparison between Predictions and Measurements

An example of predicted sonic-IR signal is given in Figure 5 c) with the corresponding measurement. Since edge effects at the crack corners were not considered, the predicted temperature rise was uniform over the width of the beams. The average temperature rise measured by the IR camera along all pixels covering the crack width was compared with the predictions for each pulse of vibration. More examples of such comparisons are shown in Figure 6 in the time domain. It can be noted that even though the shape of the predicted signal is substantially the same as the measured signal, the predictions are not always in perfect agreement with the measurements. The difference between the predictions and the measurements can be usually described by a single multiplicative factor for each test. In order to understand whether this discrepancy was the same for all tests and for all specimens, the average measured and predicted thermosonic signals (during temperature rise and fall) were plotted against each other, as illustrated in Figure 7 for 2 of the 7 specimens.

It can be seen that the predictions show a clear linear trend with the measurements, with the least squares line having different slopes for different specimens. However, perfect agreement was not always obtained as this would have been equivalent to having the plotted points laying close to the line with unit slope. Table 1 summarizes the number of tests

available for each specimen, the slopes of the fitted lines and the variability of the temperature rise measured across the width of the cracks.

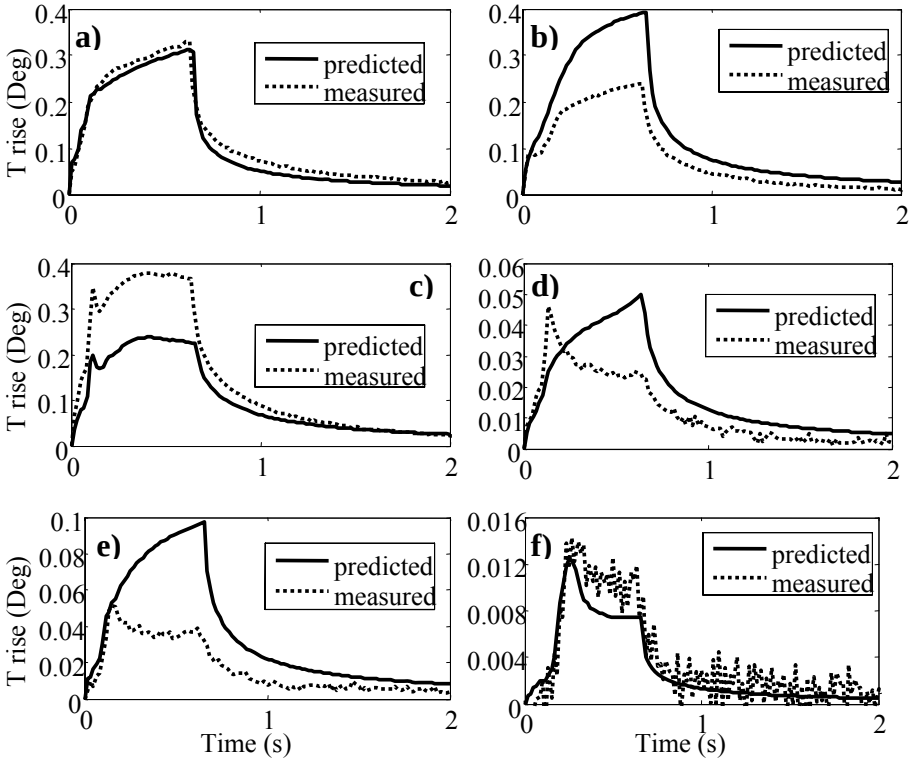

Figure 6 Examples of comparisons between measured and predicted thermosonic signals from different tests in different specimens: all the significant cases are represented. (a) specimen 1 test 16, excellent agreement; (b) specimen 3 test 15, substantial prediction overestimate with agreement in the shape of the transient; (c) specimen 6 test 17, prediction underestimate with agreement in shape; (d) specimen 7 test 9, similar maximum temperature rise but different shape of transient; (e) specimen 2 test 18, disagreement both in shape and maximum value; (f) specimen 4 test 7, barely measurable temperature rise.

The variability of the slopes of the fitted prediction-measurement lines among different specimens may be due to a different initial partial opening of the cracks, to other 3D effects at the crack that were not considered in the modelling and/or to the fact that damping measurements were available only up to 30 με whereas many thermosonics tests exceeded this level. However these comparisons showed that there was always a good linear correlation between prediction and measurements, which validated the prediction algorithm.

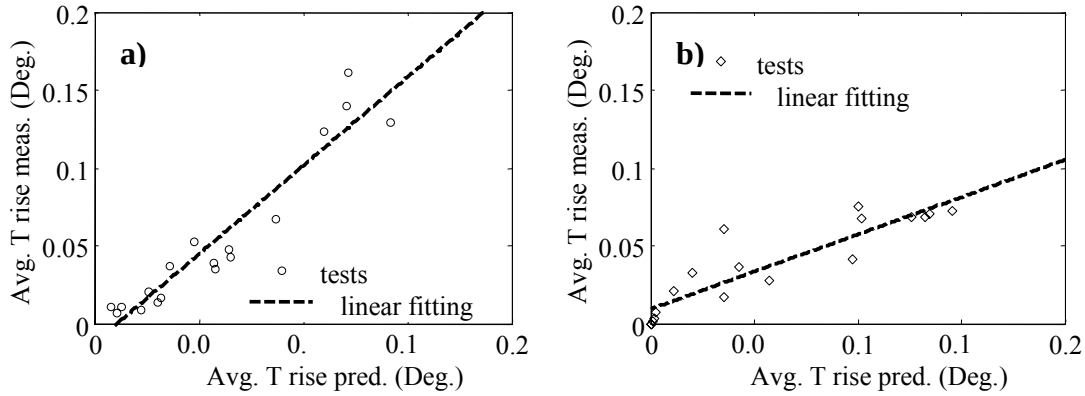

Figure 7 Average magnitude of the measured thermosonic signal vs average magnitude of the predicted thermosonic signal for all tests in specimens 1 (a) and 2 (b). The dashed line is the linear fit.

Table 1 Summary of the number of tests carried out for each specimen, the slopes of the lines fitted to the predicted vs measured temperature rises and the average variability of the temperature across the width of each crack expressed as the standard deviation divided by the mean value.

Specimen	1	2	3	4	5	6	7
number of tests	18	16	17	17	16	18	14
Slope	1.1	0.45	0.59	0.53	1.6	1.3	0.77
(σ/m) (%)	52	33	26	41	37	27	27

4. Temperature Rise vs Crack Size

The second step of the analysis of the results was a sensitivity analysis to find, if possible, the minimum detectable crack size using this implementation of the thermosonic method and the current specimens.

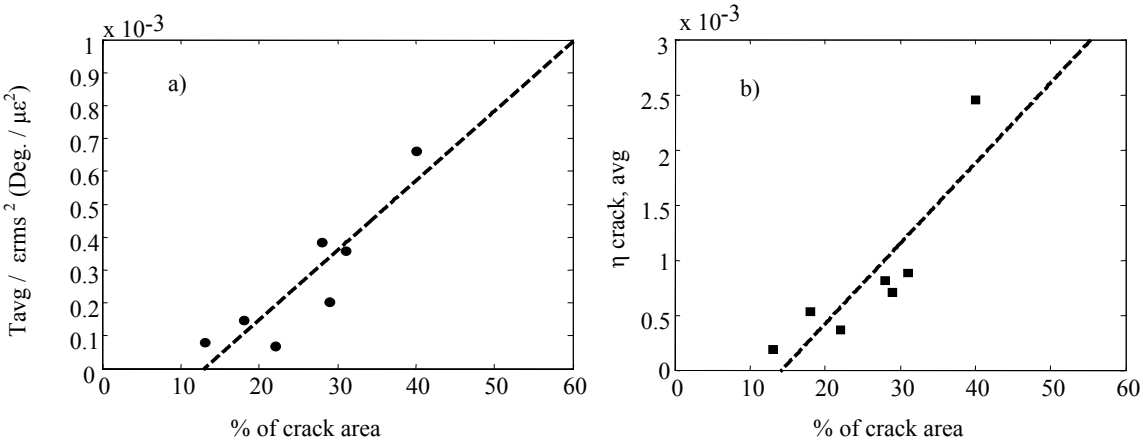

Figure 8 (a) measured average temperature rise per unit of strain squared plotted vs percentage of cracked cross section. (b) crack loss factor vs percentage of cracked cross section. The dashed lines represent the linear fit.

The amplitude and frequency content of the strain record for each test was non-stationary, hence we computed the rms value of the strain during the whole duration of each pulse (ε-rms) as the quantity to represent the intensity of vibration. The average temperature rise Tavg over the duration of each pulse was also computed. In Figure 8 a) the ratio Tavg/ ε-rms^2 (the heat generated is proportional to ε^2), averaged among all tests available for each specimen, is plotted versus the percentage cracked area for each specimen. This ratio clearly increases with increasing crack size, although there is considerable scatter in the data. It is believed that the scatter is related (1) to the different levels of initial crack partial opening which could affect the magnitude of the thermosonic signals for any given crack size and (2) to the non-uniform shape of the cracks across the width and through the depth of the specimens. The least square linear fit is also shown in Figure 8 a), and it can be seen that it does not intercept the axis near the origin. This is not physically possible, as virtually no temperature increase must correspond to the absence of a defect (an extremely small temperature rise would in theory be possible in the absence of a defect due to internal damping, but this was never measurable in our experiments). In fact the relationship between temperature rise and crack size is likely to be non-linear. A study of the

relationship between defect size and temperature rise for smaller cracks that do not propagate across the full width, which are of most interest in practice, is now needed. Figure 8 b) shows the relationship between the average crack related loss factor from figure 3 and the crack size. Unsurprisingly the trend is very similar to that of Figure 8 a) since the increase in loss factor is what produces the temperature rise.

5. Conclusions

In this paper the prediction of the temperature rise used by the thermosonic method of NDT to detect cracks in metallic structures was achieved on the basis of independent measurements of the extra damping introduced in the test specimens by the presence of the crack. Such an approach has the advantage of globally evaluating the extra losses at the crack and assumes the same extra losses to be responsible for the temperature increase close to the crack which allows detection. In this way the thermosonic signal could be related to the amplitude and frequency content of the excited vibrations, even though variable and uncontrolled coupling conditions between the horn and the specimens were responsible for the excitation of time varying vibrations.

The results reported in this study confirm that the proposed approach is promising. The vibration thresholds able to generate a thermosonic signal strong enough to be detected by the IR camera can be derived since a linear trend was found between the predicted and measured temperature rise.

References

[1] Thomas, R. L., "Thermal NDE Techniques – from Photoacoustics to Thermosonics" in *Review of Progress in Quantitative Nondestructive Evaluation 21*, edited by D. O. Thompson and D. E. Chimenti, AIP Conference Proceedings vol. 615, American Institute of Physics, Melville, NY, 2002, pp. 3-13.

[2] Pye, C. J., Adams, R. D., *Ndt & International* **14**, 111 (1981).

[3] Pye, C. J., Adams, R. D., *Journal of Physics – Applied Physics* **14**, 927 (1981).

[4] Di Favro, L. D., Thomas, R. L., Han, X. Y., Ouyang, Z., Newaz, G., Gentile, D., *International Journal of Fatigue* **23**, *S*471 (2001).

[5] Han, X. Y., Di Favro, L. D., Thomas, R. L.,"Recent Developments in Sonic IR Imaging" in *Review of Progress in Quantitative Nondestructive Evaluation 22*, edited by D. O. Thompson and D. E. Chimenti, AIP Conference Proceedings vol. 657, American Institute of Physics, Melville, NY, 2003, pp. 500-505.

[6] Zweschper, T., Dillenz, A., Busse, G., *Insight* **43**(3), 173-179 (2001).

[7] Han, X. Y., Zeng, Z., Li, W., Islam, M. S., Lu, J. P., Loggins, V., Yitamben, E., Di Favro, L. D., Newaz, G., Thomas, R. L., *Journal of Applied Physics* **95**, 3792 (2004).

[8] Han, X. Y., Loggins, V., Zeng, Z., Di Favro, L. D., Thomas, R. L., *Applied Physics Letters* **85**, 1332 (2004).

[9] Lazan, B. J., *Damping of Materials and Members in Structural Mechanics*, Pergamon Press, Oxford, 1968.

[10] Cawley, P., Sarsentis, N., *Mechanical Systems and Signal Processing* **2**, 39 (1988).

[11] Bovsunovsky, A.P., in *Engineering Fracture Mechanics* **71**(16-17), 2271 (2004).

[12] Goken, L.D., Letzig, D., Kainer, K.U., in *Journal of Alloys and Compounds* **378**, 220 (2004).

[13] Ouyang, Z., Di Favro, L. D., Thomas, R. L., Han, X. Y., .,"Theoretical Modeling of Thermosonics Imaging of Cracks" in *Review of Progress in Quantitative Nondestructive Evaluation 21*, edited by D. O. Thompson and D. E. Chimenti, AIP Conference Proceedings vol. 615, American Institute of Physics, Melville, NY, 2002, pp. 577-581.